RSMC Tokyo – Typhoon Center

Technical Review

No. 1

Contents

Japan Meteorological Agency

March 1995

An Improvement in Tropical Cyclone Bogussing for Numerical Models at the JMA

Mitsuru Ueno and Kazutoshi Onogi

Numerical Prediction Division, Japan Meteorological Agency

Abstract

Tropical cyclone bogussing procedure for numerical models at the JMA was improved. A statistical verification study revealed that the initial fields derived through the new bogussing procedure are more realistic and thus improve the prediction of tropical cyclone tracks especially in low latitudes.

1. Introduction

Data sparsity over the ocean is a long-pending problem for the analyses of tropical cyclones because they remain in the ocean areas during most of their lifetimes. Scarce data even make the initial vortex structure for numerical models unrealistic and deteriorates their capability in tropical cyclone forecasting as a result. Bogus observations (*e.g.* geopotential heights and wind velocities) are therefore introduced in order to compensate for the lack of data and thereby fix more appropriate initial fields for the numerical models.

An outline of the JMA operational forecast system is given by Kitade (1988). The bogussing aspects of the system are described in greater detail. As for the operational typhoon numerical forecasts, the bogussing techniques carried out in the general-purpose forecast models (*e.g.* global spectral model) and the typhoon track prediction model (TYM) are described by Ueno (1989).

On 3 September 1991, the JMA improved the operational procedure for tropical cyclone bogussing. In the new bogussing procedure, the formula to determine the pressure profiles of storms was modified and actual surface observations were employed to correct the profile given by the formula. This paper gives a brief summary of the improvement and its impact on tropical cyclone forecast by the operational numerical models of the JMA.

2. The improvement in the bogussing procedure

Bogus observations are employed in the tropical cyclone analysis of the assimilation system when a tropical cyclone exists within the area of the JMA's responsibility, north of the equator from 100°E to 180°. The general procedure for the tropical cyclone analysis is outlined as below:

Step-1   To fix the storm size using the objectively-analyzed radius of over 30-knot winds area;

⇓

Step-2   To generate bogus data from the storm size and objectively-analyzed central pressure with empirical formulae;

⇓

Step-3   To perform pre-analysis to revise the
first guess field using only the bogus
data; currently, prognosis of the Global
Spectral Models is used operationally
as the first guess field;

⇓

Step-4   To perform objective analysis for the
revised first guess field.

Note that the bogus data are not used in the objective analysis but used in the pre-analysis exclusively to revise the first guess field. In this improvement, primary changes were made in the Step-1 and -2, and are briefed as follows:

(1) The following basic (Fujita's) formula was adopted to represent an axis-symmetric sea-level pressure (SLP) pattern of a tropical cyclone as a function of r (radial distance from the center).

$$P(r) = P_\infty - (P_\infty - P_c)\{1 + (r/R_o)^2\}^{-1/2}$$

where P_∞ is the SLP at infinite distance, P_c is the central pressure, and R_o is the parameter to prescribe the SLP profile of a tropical cyclone.

(2) R_o is determined from the gradient wind relation by introducing pressure gradients derived from Fujita's formula and the analyzed wind profile.

(3) The SLP profile is rectified by synoptic surface observations by use of the least-squares-fitting method when five synoptic reports or more are available in the cyclone's vicinity.

(4) The central pressure was increased to be adapted to the horizontal resolution of the objective analysis for preventing the initial fields from being distorted by the extreme pressure gap between the inner and outer region of the cyclone.

(5) 100 hPa level was adopted instead of 150 hPa level of the former version, where the positive anomaly of temperature within the cyclone become zero while it reaches the maximum at 250 hPa level (at 300 hPa level in the former version).

(6) Bogus observations were increased in the number in such a manner as to make the observation density uniform in space.

3. Impact of the changes

Bogus observations derived by the current and former methods are compared with real observations in Figure 1. The mean bias errors and their root-mean-square in the figure imply the current method has significantly improved the bogus cyclone in its consistency with

the real one particularly in lower troposphere. However, the errors are still relatively large in upper troposphere mainly due to the increase of asymmetry in the wind fields of storms (for this reason bogus observations are used only for the middle and lower troposphere at the pre-analysis).

Tables 1 and 2 present a summary of track forecast errors of Global Spectral Model (GSM) and Asia Spectral Model (ASM) for some of the tropical cyclones in 1990 and 1991; As shown in the tables, the improvement in the bogussing procedure is apparently reflected in the forecast performances. It is more explicit in Figure 2 where the forecast errors in both cases are comparatively displayed as triangles in scatter diagrams; the triangle in the upper side of the dashed line indicates that the NEW method outperforms the OLD one.

Further comparisons were made between the two methods. In Figure 3, the forecast tracks of Severe Tropical Storm GLADYS (9112) by GSM and those of Typhoon PERCY (9006) by ASM based on the old and new bogussing methods are shown with their best tracks. In both the cases the method adopting the new bogus field demonstrated improvements upon track forecast. In addition, Figure 3-(b) shows the mitigation of the northward bias that is frequently observed in the models' forecast of tropical cyclone tracks in low latitudes Ueno (1989).

4. Concluding Remarks

For the more accurate forecast of tropical cyclones, it is crucial to provide numerical models with more realistic initial vortices along with improvements in models' physical processes. Above results prove the importance of description of axis-symmetric wind components of tropical cyclones and the effectiveness of employing actual observations in initial fields. Therefore, it is fully expected that new information about the satellites observations such as that by microwave sounders will make further contributions to the improvements of model's performance in tropical cyclone forecasting. Above results prove the effectiveness of more precise description of axis-symmetric wind components of tropical cyclones and hence suggest that it is crucial to provide numerical models with more realistic initial vortices for the more accurate forecast of tropical cyclones.

REFERENCES

Kitade, T., 1988: Numerical Weather Prediction in Japan Meteorological Agency. JMA/NPD *Tech. Rep., No. 20, Japan Meteorological Agency.*

Ueno, M., 1989: Operational bogussing and numerical prediction of typhoon in JMA. *JMA/NPD Tech. Rep., No. 28, Japan meteorological Agency.*
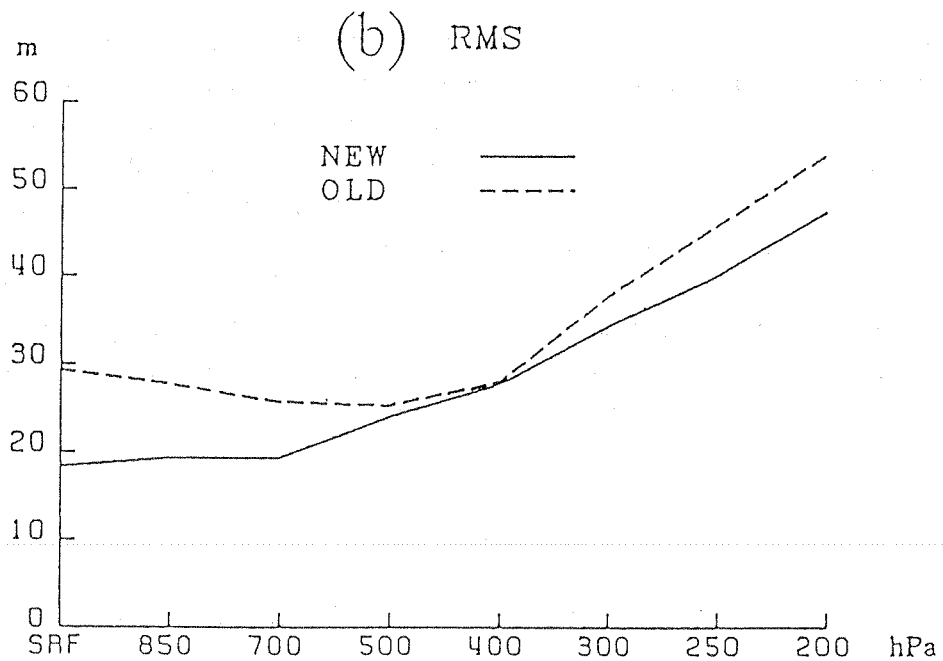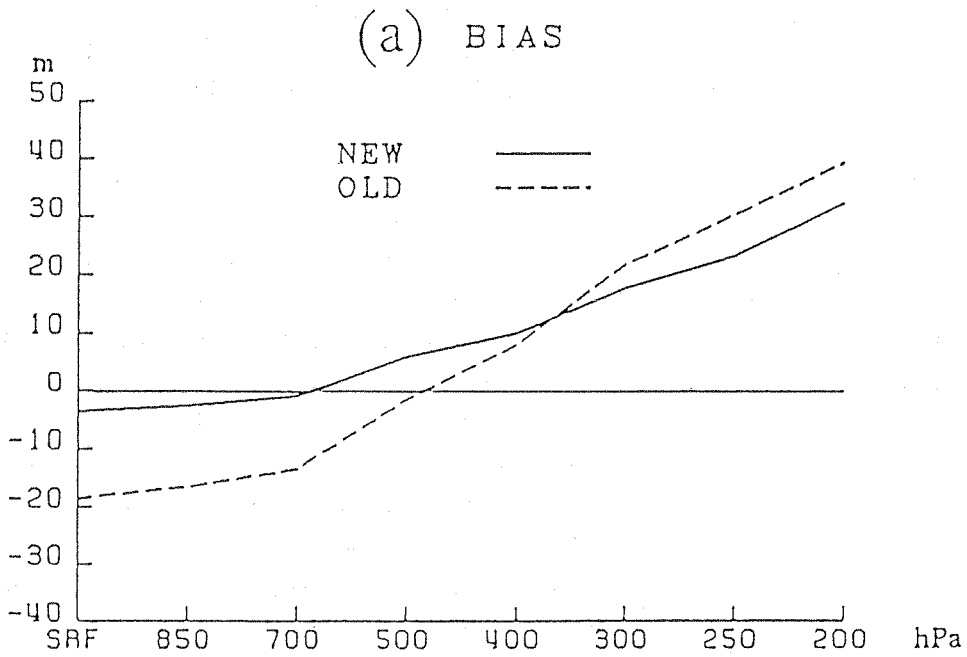
Fig. 1. (a) Mean differences in isobaric height (m) between bogus observations and real observations as a function of vertical levels (abscissa); bogus observations are derived through the current (NEW) and former (OLD) bogussing method. (b) Same as (a) but root mean square of the differences.
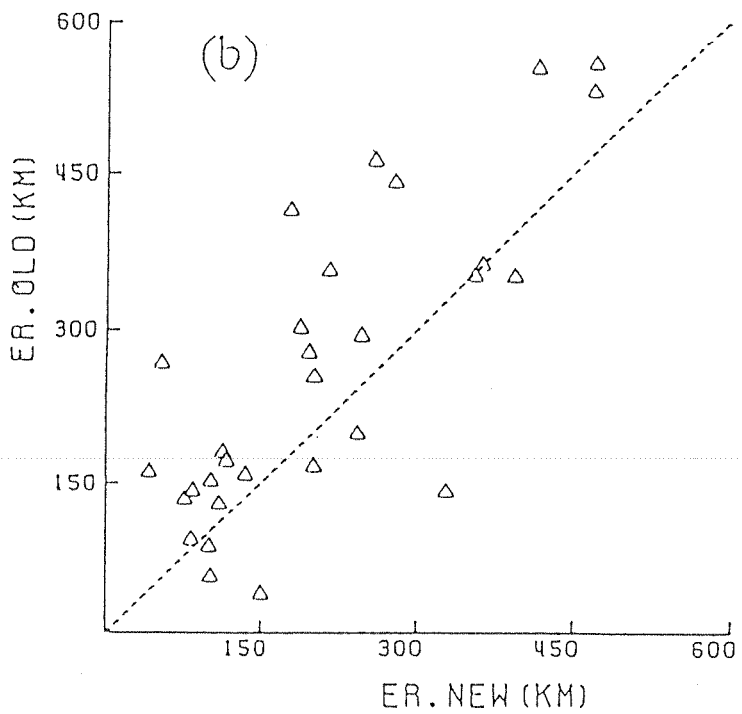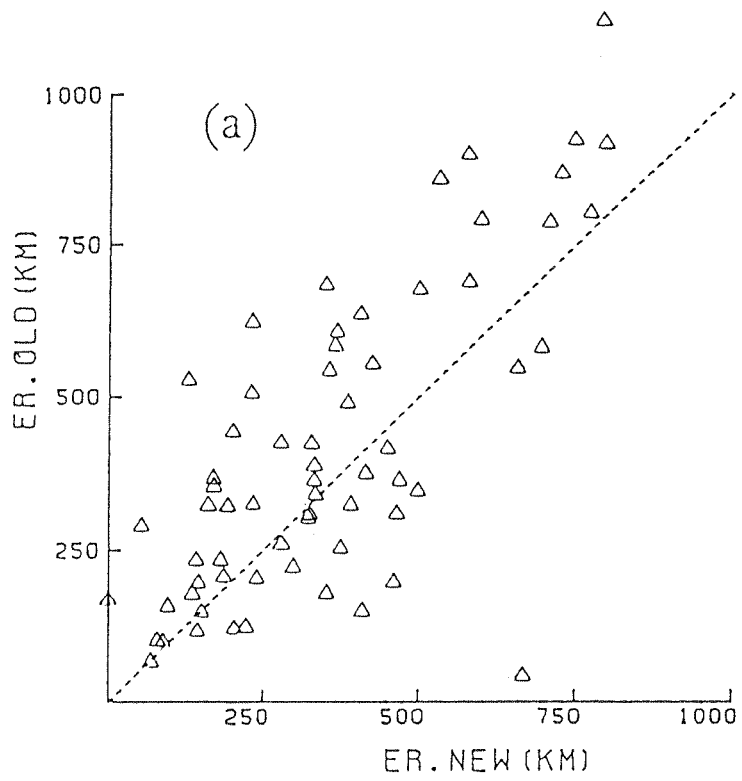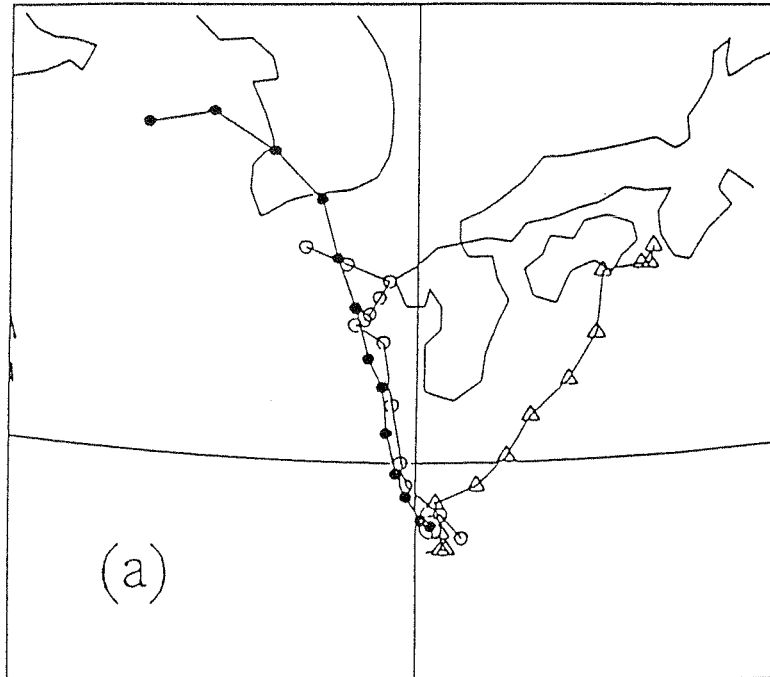
Fig. 2. Scatter diagram of the errors for 48-hour forecasts by (a) GSM and (b) ASM using NEW and OLD bogussing method.

STS 9112 GLADYS
INITIAL TIME : 0000 UTC 21 AUG 1991
FORECAST PERIOD : 0 - 72 HOURS

(a)

TY 9006 PERCY
INITIAL TIME : 0000 UTC 27 JUN 1990
FORECAT PERIOD : 0 - 48 HOURS

(b)
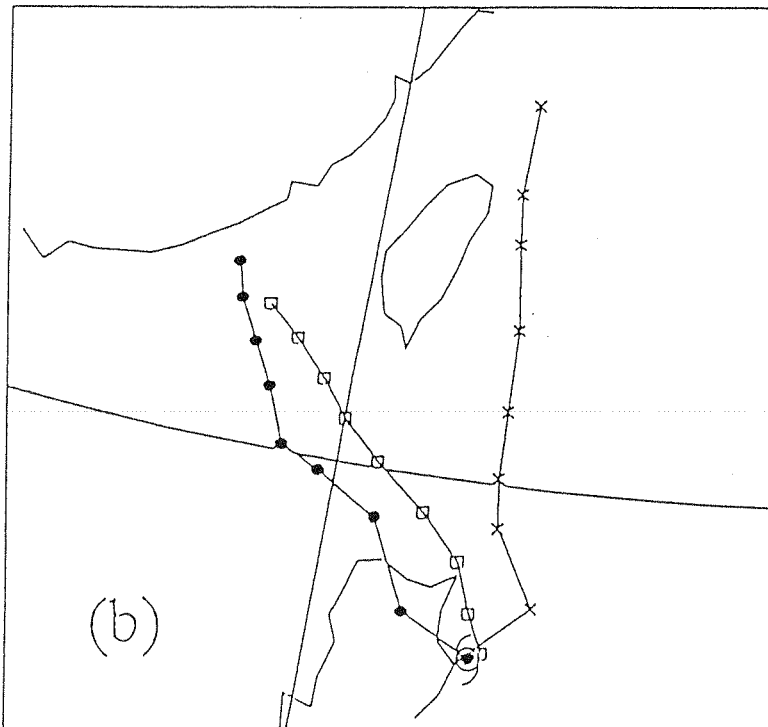
Fig. 3. Track forecast examples. (a) 72-hour forecast track of STS 9112 GLADYS by GSM using
OLD bogussing method (marked with triangles at 6-hour intervals) and NEW one (with open
circles). Best track is marked with solid circles. (b) 48-hour forecast track of TY 9006 PERCY
by ASM using OLD bogussing method (marked with slant crosses at 6-hour intervals) and
NEW one (with squares).

Table 1. Mean forecast errors (km) for GSM using OLD and NEW bogussing method. The number of cases is in parentheses.

TROPICAL CYCLONE	BOGUS	T=12	T=24	T=36	T=48	T=60	T=72
TY 9006 PERCY	OLD	265 (7)	414 (6)	630 (6)	862 (6)	1145 (5)	1463 (5)
	NEW	162 (7)	313 (6)	488 (6)	660 (6)	862 (5)	1110 (5)
TY 9008 STEVE	OLD	375 (1)	673 (1)	923 (1)	1118 (1)	1207 (1)	998 (1)
	NEW	279 (1)	519 (1)	708 (1)	792 (1)	647 (1)	584 (1)
TY 9010 VERNON	OLD	86 (11)	148 (11)	214 (11)	256 (10)	337 (10)	471 (7)
	NEW	82 (11)	135 (11)	208 (11)	240 (10)	334 (10)	464 (7)
TY 9018 ED	OLD	122 (5)	193 (5)	275 (5)	382 (5)	476 (5)	585 (5)
	NEW	102 (5)	146 (5)	206 (5)	291 (5)	382 (5)	444 (5)
TY 9019 FLO	OLD	126 (5)	213 (5)	294 (5)	380 (5)	462 (4)	215 (3)
	NEW	105 (5)	186 (5)	296 (5)	417 (5)	565 (4)	409 (3)
TY 9104 WALT	OLD	122 (18)	213 (18)	303 (18)	413 (16)	521 (14)	659 (13)
	NEW	109 (18)	177 (18)	265 (18)	346 (16)	432 (14)	563 (13)
TY 9109 CAITLIN	OLD	122 (6)	183 (6)	264 (6)	365 (6)	553 (6)	687 (5)
	NEW	106 (6)	177 (6)	284 (6)	404 (6)	614 (6)	652 (5)
TY 9110 ELLIE	OLD	147 (9)	250 (7)	358 (5)	385 (4)	388 (4)	369 (4)
	NEW	113 (9)	224 (7)	281 (5)	313 (4)	381 (4)	491 (4)
TY 9111 FRED	OLD	69 (4)	139 (4)	188 (4)	175 (4)	281 (3)	371 (3)
	NEW	102 (4)	91 (4)	74 (4)	217 (4)	124 (3)	173 (3)
STS 9112 GLADYS	OLD	142 (9)	206 (9)	312 (9)	411 (8)	514 (8)	675 (7)
	NEW	112 (9)	151 (9)	205 (9)	276 (8)	351 (8)	490 (7)
MEAN	OLD	136 (75)	221 (72)	318 (70)	415 (65)	527 (60)	651 (53)
	NEW	112 (75)	182 (72)	264 (70)	353 (65)	449 (60)	553 (53)

Table 2. Same as Table 1 but ASM.

TROPICAL CYCLONE	BOGUS	T=12	T=24	T=36	T=48
TY 9006 PERCY	OLD	295 (6)	463 (6)	543 (6)	592 (5)
	NEW	210 (6)	326 (6)	381 (6)	417 (5)
TY 9010 VERNON	OLD	113 (2)	203 (2)	292 (2)	406 (2)
	NEW	106 (2)	153 (2)	231 (2)	316 (2)
TY 9104 WALT	OLD	165 (5)	249 (5)	326 (5)	400 (5)
	NEW	122 (5)	194 (5)	256 (5)	308 (5)
TY 9109 CAITLIN	OLD	44 (1)	93 (1)	323 (1)	542 (1)
	NEW	90 (1)	83 (1)	169 (1)	318 (1)
TY 9110 ELLIE	OLD	229 (7)	288 (6)	288 (5)	337 (4)
	NEW	192 (7)	292 (6)	308 (5)	426 (4)
TY 9111 FRED	OLD	70 (3)	105 (3)	140 (3)	212 (3)
	NEW	91 (3)	104 (3)	117 (3)	153 (3)
STS 9112 GLADYS	OLD	104 (7)	174 (7)	242 (7)	335 (7)
	NEW	70 (7)	128 (7)	184 (7)	290 (7)
MEAN	OLD	175 (31)	259 (30)	322 (29)	394 (27)
	NEW	138 (31)	209 (30)	255 (29)	325 (27)

Estimation of Vertical Moisture Profiles from GMS Cloud Data

Atsushi Baba

Numerical Prediction Division, Japan Meteorological Agency

Abstract

An algorithm for moisture estimation from GMS (Geostationary Meteorological Satellite) cloud data adopted by the JMA (Japan Meteorological Agency) is presented. The satellite-derived moisture data have been utilized in routine moisture analyses at the JMA since 1983. In the algorithm, cloud conditions are classified into 320 categories in reference to the GMS cloud data such as cloudiness and cloud-top equivalent black body temperatures (T_{BB}) together with synoptic observations, and a typical moisture profile is determined for each of the categories based on the statistical relationship. Thus, vertical moisture profiles are objectively estimated as a function of the cloud condition.

1. Introduction

Moisture is one of the most important atmospheric parameters for numerical weather prediction (NWP) models. Special emphasis is accordingly put on the moisture analysis in order to obtain more accurate initial moisture fields, which is critical, *inter alia*, for rainfall forecast. However, radiosonde observations are not abundant enough to analyze moisture fields with a sufficient resolution, being too sparsely distributed especially over the ocean. Retrieval of moisture profiles from other observations has therefore been attempted to supplement the meagerness of the moisture data.

Smith and Howell (1971), Hayden *et al.* (1981), and Lipton *et al.* (1986) developed procedures to retrieve water vapor profiles from satellite measurements. Chisholm *et al.* (1968) investigated the relationship between surface synoptic observations and the collocated TEMP data and thus developed a diagnostic approach to estimate humidities at standard pressure levels (850 hPa, 700 hPa, 500 hPa, and 400 hPa) from surface observations. Jonas (1976) demonstrated that the upper moisture data estimated from surface observations have considerable availability for the upper level humidity analysis. Thompson and West (1967), Smigielski and Mace (1970), Walcott and Warner (1981), and Mills (1983) used cloud imageries observed by meteorological satellites to estimate water vapor fields. Walcott and Warner (1981) applied satellite cloud data to moisture analysis based on the assumptions as follows: if precipitation is observed at the surface, relative humidity is 100% from the surface to the cloud top level; if not, it is 100% only at the cloud top level. They showed that these supplementary data allowed NWP models to improve the forecast of rainfall intensity.

In light of these studies as above, the JMA established a scheme to estimate vertical moisture profiles from GMS cloud data and put it into the routine moisture analysis in 1983 (revised in 1988). In this scheme, the vertical profile of relative humidity is determined as a function of the GMS cloud data based on the statistical relationships between the GMS cloud data and the actual measurements of moisture. We hereafter call the moisture profile estimated from the GMS cloud data as "GMS moisture data".

2. GMS cloud data

The GMS cloud data, which are derived from the GMS observations at 00, 06, and 12 UTC, consist of several parameters representing cloud conditions such as cloudiness and cloud–top equivalent black body temperatures (T_{BB}) in each $0.5° \times 0.5°$ latitude/longitude within the area of 50°N–50°S, 90°E–170°W (see Table 1).

A set of these parameters allows of objective estimation of the cloud conditions at each mesh. For example, i) the cloudiness of 100% at a mesh immediately means that the grid is filled with clouds, ii) the relatively high (low) mean T_{BB} indicates predominance of low–level (high–level) clouds, and iii) the large (small) standard deviation of T_{BB} suggests cumuliform (stratiform) clouds. Also, the cloud condition inferred at a mesh gives a rough image of a vertical moisture profile at the mesh. For example, if the cloudiness is 100 %, the mean cloud–top level estimated from T_{BB} is 700 hPa and the standard deviation of the T_{BB} is 1 K, the atmosphere above 700 hPa is considered to be dry while that of below 700 hPa be wet. Thus, the GMS cloud data roughly profile the vertical distribution of moisture.

3. Classification of cloud condition and retrieval scheme

In order to apply most appropriate vertical profiles of moisture, cloud conditions are classified into numbers of categories with three parameters of the GMS cloud data; those parameters are 1) cloudiness, 2) mean cloud–top height converted from the mean T_{BB} in reference to the analyzed temperature profile or the first guess temperature, and 3) standard deviation of T_{BB}.

Among these three parameters, the cloudiness displaying the general moisture condition of a mesh is divided into five classes, i.e., 0%, 1–20%, 21–70%, 71–99%, and 100%. The mean cloud–top height which gives the height of the uppermost moist atmosphere is divided into six levels when the cloudiness is more than 20%, i.e., 300 hPa or higher, 301–400 hPa, 401–500 hPa, 501–700 hPa, 701–850 hPa, and lower than 850 hPa. Also, the standard deviation of T_{BB} indicative of the type of cloud is divided into two classes when the cloudiness is greater than 70%: less than 3K, which means that clouds are stratiform and so the moisture gradient is generally sharp between cloud and cloud–free layers; and 3K or greater, which means that clouds are cumuliform and so the moisture gradient is moderate between the layers. Consequently, as shown in Table 2, the cloud conditions are classified into the 32 categories.

However, since the GMS cloud data describes the atmospheric conditions only above the cloud–top, synoptic reports which offer weather conditions (or moisture conditions below the cloud–base) are incorporated into the classification for the more realistic moisture profile. For example, it can be estimated that the whole layer from the cloud–top down to the surface is wet when precipitation is observed at the surface, while wet is only the layer from the cloud–top to the cloud–base when no precipitation is observed. In order to affiliate with the information, weather conditions are classified into five categories, "rain"; "rain in the past 3 hours or in the vicinity"; "no rain"; "high cloud–base" (cloud–base is higher than 2000 m above the surface); and "unknown" (no synoptic report is available). In addition, because humidity in the tropics is generally higher than in the extratropics, the locations of meshes are divided into two groups according to their latitudes, i.e., those in 23.5°N–23.5°S (tropical region) and in 23.5°N–50°N/23.5°S–50°S (subtropical region). Eventually, the above 32 categories of cloud conditions are classified further into 320 sub–categories by the

combination of the five weather categories and the two regional groups.

For each of these categories, vertical moisture profiles are statistically deduced from the radiosonde data observed under the corresponding cloud conditions. In the statistics, the average radiosonde–observed profiles were defined as the estimated vertical moisture profiles, and their standard deviations (σ_R) are defined as the errors of the estimation to be used as the observation errors in the objective analysis.

Examples of the derived profile of moisture and standard deviation are shown in Table 3 and Figure 1. In this case, the cloud condition is classified as the category number 12, where the cloudiness is 71–99%, the mean cloud–top height is more than 700 hPa and less than 500 hPa, the standard deviation of T_{BB} is smaller than 3K, and the weather category is "rain". These parameters indicate that the region is mostly covered with stratus with cloud–top existing between 700 hPa and 500 hPa levels and that the precipitation is observed at the surface. The moisture profile presented in Figure 1 exhibits the wetness below 700 hPa to the surface and dryness above 700 hPa, being consistent with the moisture profile presumable from this category of cloud condition.

In addition, because some of the errors in statistically derived moisture profiles as shown above could be less than the systematic error of radiosonde observation, 5%, we employed σ_G instead of σ_R expressed by

$$\sigma_G = \sqrt{(\sigma_R)^2 + (5\%)^2}$$

to be used in the objective analysis.

The operational procedure to obtain GMS moisture data is briefed as follows (the schematic flow of the procedure is illustrated in Figure 2).

(1) The category number for a cloud condition at each mesh is determined from the GMS cloud data and temperature analyses are needed to convert the T_{BB} to the cloud–top height.

(2) The category number for the weather condition is determined from the synoptic report.

(3) With these category numbers, a vertical profile of moisture is given for the mesh and used in the objective analysis along with estimation errors (or observation errors) at standard pressure levels as the moisture data at the data point; the "data point" is defined as the point where the surface observation was carried out, or the center of the mesh when no observation is available.

Thus, the GMS cloud data, together with the surface observations, approximate the vertical distributions of moisture and thereby afford objective analysis realistic moisture fields, which are absolutely effective in the regions where very few radiosonde observations are available.

4. Impact of the GMS moisture data on numerical prediction

Figure 3 illustrates the moisture analysis at 700 hPa level at 12 UTC on 24 July 1989 and the GMS cloud data at the same time when a tropical cyclone is located to the south of

Japan. Shaded in the Figure 3-(a) are the areas with relative humidity of 80% or more (or T-Td of 3°C or less). Radiosonde data and GMS moisture data are indicated by "∗" and "×"/"+"), respectively, where "×" indicates the data derived with surface observations and "+" without surface observations. Note that the GMS moisture data are produced only for the oceanic areas and not for the land areas where the radiosonde data are relatively abundant and GMS data are deteriorated.

Basically, GMS moisture data are produced with the density of one in every 2° latitude-longitude grid. In addition, reliability of the GMS moisture data determined with the surface observations take precedence of those without surface observations. Further, the GMS moisture data are not produced within 300 km from the radiosonde observations. It is because that the accuracy of the GMS cloud data are not satisfactory over the land. Comparing the Figure 3.(a) to 3.(b), one can find that the moisture field in Figure 3-(a) is quite reasonable with the well demonstrated moist area accompanied by the tropical cyclone.

In Figure 4, GMS cloud imagery at 00 UTC 27 July 1988 is presented. The three figures on the left of Figure 5 are the objective moisture analyses at 500 hPa, 700 hPa and 850 hPa levels at the same time. It should be noted that the three zonal cloud systems around latitudes of 40°N, 20°N and the equator shown in Figure 4 are analyzed consistently in Figure 5 even though radiosonde data are sparse or non-existent in most of these regions. The three figures on the right of Figure 5 are shown the objective moisture analyses without GMS moisture data; the results of the forecast-analysis cycle conducted for the last seven days without the GMS data. Note that the zonal cloud systems, in particular that around 20°N in latitude, and the cloud free regions are not clear in these figures.

As indicated in these cases, the GMS moisture data allow the objective analysis to analyze moisture fields fairly accurately over radiosonde-data sparse ocean areas, providing realistic moisture distributions in the synoptic-scale cloud systems such as tropical cyclones and ITCZ. More specifically, such data bring out the sharp moisture contrast between the cloud and cloud-free regions in initial fields of numerical models, and lead to the more reasonable difference of precipitation potential between those two regions, thus having a significant impact on the models' forecast performances, on the precipitation forecast in particular.

5. Summary and remarks

Vertical moisture profiles are objectively estimated from GMS cloud data with predetermined profiles typical to the cloud conditions, which were derived based on the statistical relationships. In the estimation process, moisture conditions are classified into 320 categories with synoptic reports and cloud conditions determined by the GMS cloud data such as cloudiness and T_{BB}, and a vertical moisture profile typical to each category is given by the statistics. Thus, upper moisture data are objectively estimated as a function of the cloud condition defined by the GMS cloud data.

GMS moisture data are quite useful in moisture analysis and precipitation forecast, particularly in the tropical oceans. But we should note that they are not capable of describing moisture profiles in detail since they are derived through statistical procedures. For example, when cirrostratus exist in the upper level while low level clouds exist with precipitation, the GMS moisture data will indicate that the all levels are wet even if the middle level is actually

dry.

An isolated radiosonde observation may represent the moisture condition at a point. When we consider that the radiosonde data represent the moisture conditions only along their passage, a large difference in moisture observation could occur depending on the radiosonde passage in the area where there are sharp contrasts in moisture distribution, e.g., inside and outside a cumulonimbus.

It is not easy to conclude which is the fair representative of moisture distribution in that particular region. Nevertheless, the effectiveness of the data are evident especially from the standpoint of the synoptic analysis of moisture field. The GMS moisture data could represent synoptic scale moisture fields, although they are not suitable for representing such small scale moisture fields as the meso-scale moisture field. Therefore, it is concluded that the GMS data give invaluable information when they are used for the synoptic-scale analysis to compensate for the lack of radiosonde data.

REFERENCES

Chisholm, D.A., J.T. Ball, K.W. Veigas, and P.U. Luty, 1968: The diagnosis of upper-level humidity, *J. Appl. Meteor.*, **7**, 613–619.

Hayden, G.M., W.L. Smith, and H.M. Wolf, 1981: Determination of moisture from NOAA polar orbiting satellite sounding radiations, *J. Appl. Meteor.*, **20**, 450–466.

Jonas, P.R., 1976: The use of surface synoptic data to estimate upper-level relative humidity over the sea, *Meteor. Mag.*, **105**, 44–56.

Lipton, A.E., D.W. Hillger and T.H.V. Haar, 1986: Water vapor vertical profile structures from satellite data via classification and discrimination, *Mon. Wea. Rev.*, **114**, 1103–1111.

Mills, G.A., 1983: The sensitivity of a numerical prognosis to moisture detail in the initial state, *Aust. Met. Mag.*, **31**, 111–119.

Smigielski, F.J., and L.M. Mace, 1970: Estimating mean relative humidity from the surface to 500 millibars by use of satellite picture, ESSA Tech. Memo. NESCTM, 23, pp.12.

Smith, W.L., and H.B. Howell, 1971: Vertical distributions of atmospheric water vapor from satellite infrared spectrometer measurements, *J. Appl. Meteor.* **10**, 1026–1034.

Thompson, A., and P.W. West 1967: Use of satellite cloud pictures to estimate average relative humidity below 500mb, With application to the Gulf of Mexico area, *Mon. Wea. Rev.*, **95**, 791–798.

Walcott, S.W. and T.T. Warner, 1981: A moisture analysis procedure utilizing surface and satellite data, *Mon. Wea. Rev.*, **109**, 1989–1998.

Table 1. GMS cloud data (Original)
Region : 50N–50S / 90E–170W
Resolution : 0.5 x 0.5 degree

Data No.	Item		Unit	Remarks
1	Cloudiness	-400 hPa		
2		400-500 hPa		
3		500-600 hPa	%	
4		600-700 hPa		
5		700-		
	Cloud-top temperature			For cloud pixel
6	Mean			
7	Minimum		K	
8	Standad Deviation			

Table 3. An example of GMS moisture data.

Category No. 12
Cloudiness   71 – 99%
Mean Cloud Top Height   501 – 700 hPa
Standard Deviation of   0.0 – 2.9K
  Cloud Top Temperature
Weather Category   Rain
Region   Tropics (23.5N – 23.5S)

Height (hPa)	Relative Humidity (%)	σ_R (%)	σ_G (%)
300	22.2	9.5	10.7
400	19.5	12.5	13.7
500	19.4	13.8	14.7
600	28.6	15.8	16.6
700	87.5	13.3	14.2
800	89.5	7.2	8.8
850	90.1	5.9	7.7
924	92.3	4.6	6.8
1000	88.7	7.4	8.9

σ_G = Observation errors. σ_R = Standard Deviation.

Table 2. Classification of cloud conditions

No.	Cloudiness (%)	Mean Cloud Top Height (hPa)	Standard Deviation (K)
1	0	-	-
2	1-20	-	-
3	21-70	-300	-
4		301- 400	
5		401- 500	
6		501- 700	
7		701- 850	
8		851-	
9	71-99	-300	0.0-2.9
10		301- 400	
11		401- 500	
12		501- 700	
13		701- 850	
14		851-	
15		-300	3.0-
16		301- 400	
17		401- 500	
18		501- 700	
19		701- 850	
20		851-	
21	100	-300	0.0-2.9
22		301- 400	
23		401- 500	
24		501- 700	
25		701- 850	
26		851-	
27		-300	3.0-
28		301- 400	
29		401- 500	
30		501- 700	
31		701- 850	
32		851-	
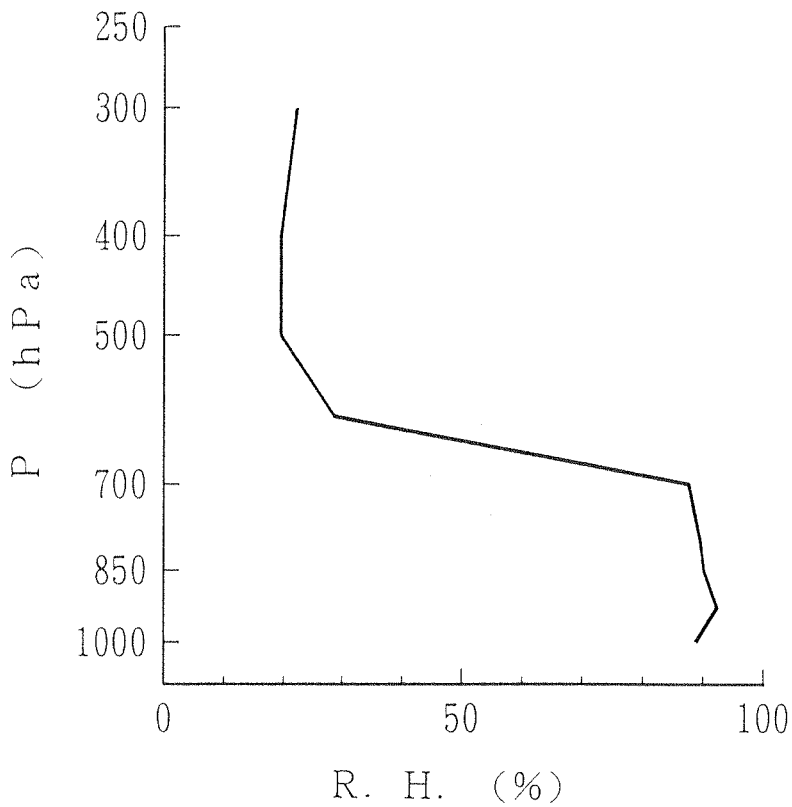
Fig. 1. An example of GMS moisture data. The vertical profile of category 12 (Graphical representation of Table 3).
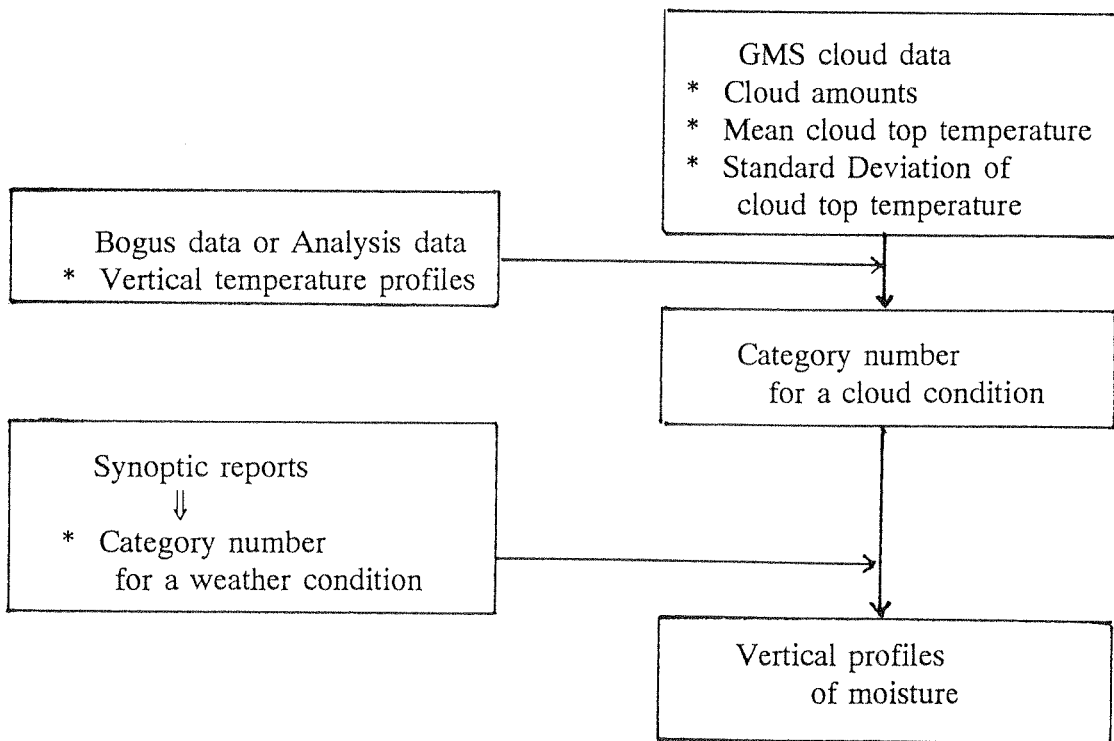
Fig. 2. The operational procedure to obtain GMS moisture data.
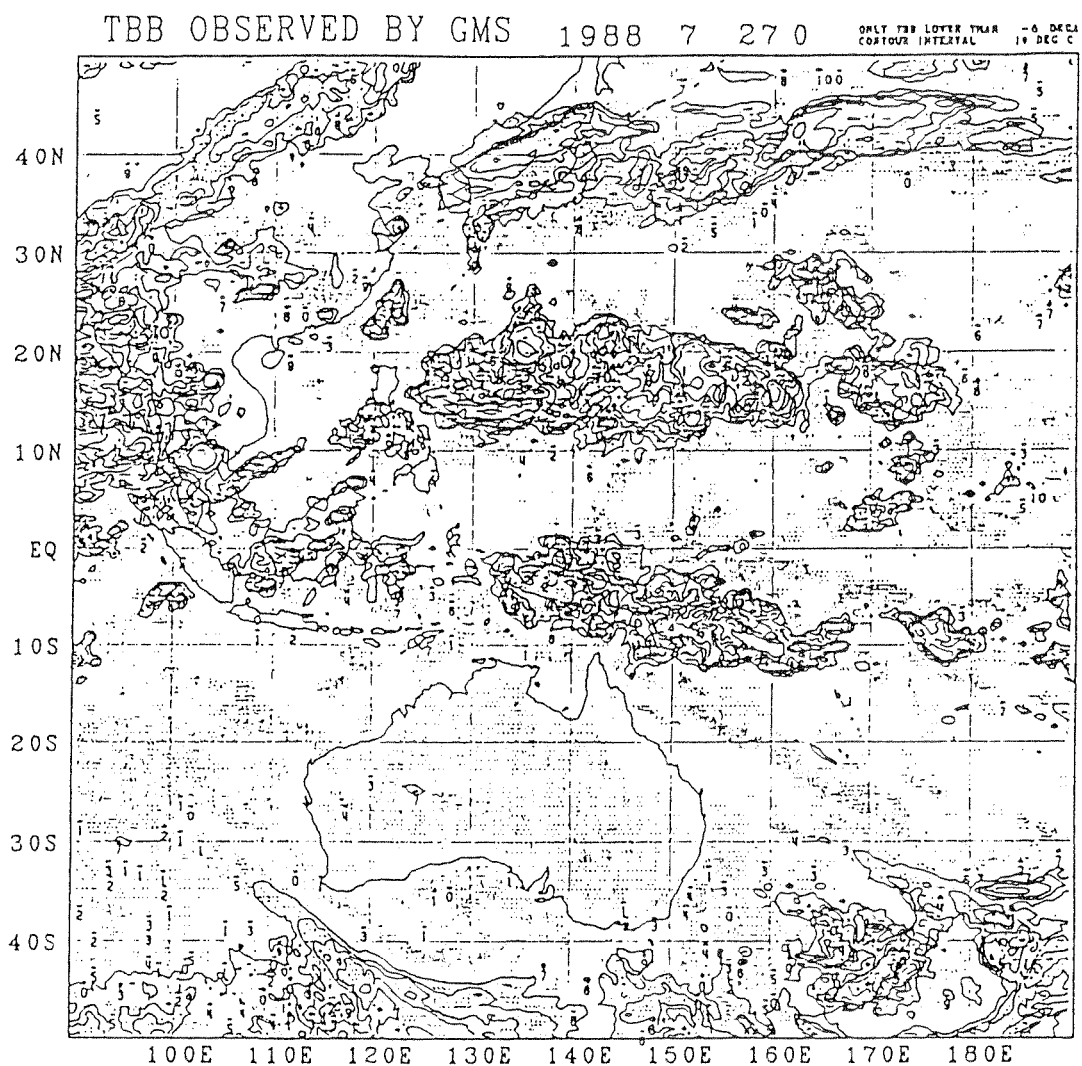
Figure 4.
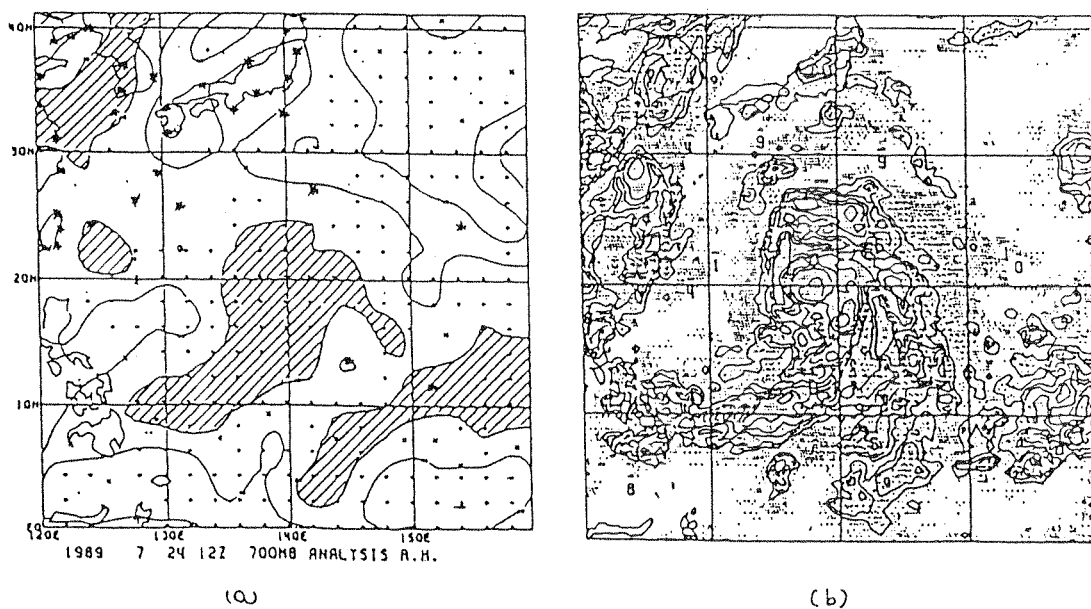
Figure 3. (a): 700 hPa moisture field analysis at 12 UTC 24 July 1989.
(b): Tbb field observed by GMS. Time/day are the same as (a).

1988　7 27 00Z 500hPa analysis

1988　7 27 00Z 500hPa analysis

1988　7 27 00Z 700hPa analysis
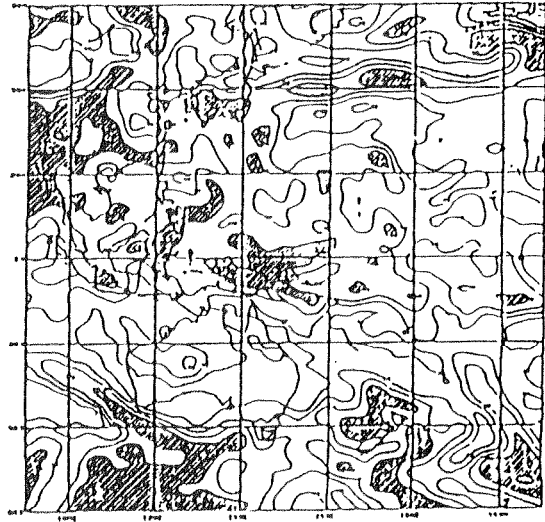
1988　7 27 00Z 700hPa analysis
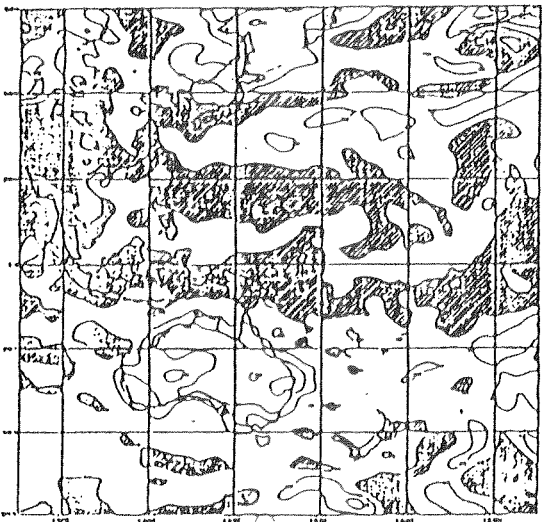
1988　7 27 00Z 850hPa analysis
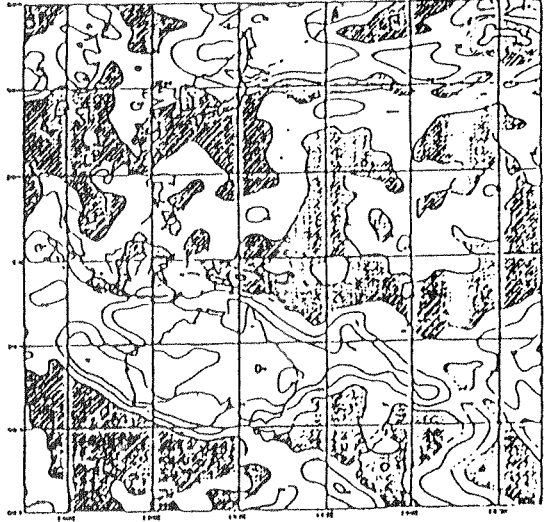
1988　7 27 00Z 850hPa analysis

Figure 5. On the left are moisture fields that are objectively analyzed using GMS data.
On the right are moisture fields, not referred to GMS data in objective analysis.
Upper: 500 hPa level, middle: 700 hPa level, Bottom: 850 hPa level.

Prediction of Cyclone Pairs by Global Spectral Model of JMA
– A Case Study with the Cyclone Pair Formed in January 1992 –

Shoji Kusunoki

Numerical Prediction Division, Japan Meteorological Agency

Abstract

A pair of tropical cyclones (or a cyclone pair) formed in January 1992 was successfully predicted by the global spectral model of JMA (Japan Meteorological Agency). This study examines the capability of the model in tropical cyclone forecasting with their occurrence, and discusses the relationship between cyclone pairs and El Niño/Southern Oscillation (ENSO).

1. Introduction

Increase in resolution, along with improvements in initial fields and cumulus parameterization, is of critical importance for numerical models to attain the higher accuracy of tropical cyclone forecast (Krishunamurti and Oosterhof, 1989; Krishunamurti et al., 1989). Although the horizontal resolution of JMA's current global prediction model (GSM; Global Spectral Model), 100 km, is not fine enough for the forecast of typhoons, substantial improvements have been achieved as compared with the former global model of which the resolution was 180 km. Bengtsson (1993) reported that a 100 km–resolution global model at Max–Planck–Institut für Meteorologie had the capability of climatological simulation of tropical cyclone occurrence. Iwasaki (1991) suggested the possibility of further improvement in typhoon track forecast utilizing an experimental global model which has a resolution of about 50 km.

Operationally, JMA has employed Numerical Typhoon Model (TYM), a limited–area model with a resolution of about 50 km, as a principal model for tropical cyclone forecast. However, limited–area models are spatially restricted; TYM is not adequate to deal with interaction between two cyclones or more. Further, the integration of those models is limited in time due to the inevitable effect of the lateral boundary of which the conditions are from global models. Global models are therefore more practical for operational tropical cyclone forecast if their resolutions are sufficiently increased.

The purpose of this study is to examine the potential ability of the current GSM in tropical cyclone forecasting.

2. Cyclone Pairs Represented by the Global Analysis of JMA

A pair of tropical cyclones that symmetrically form over the Pacific ocean in the Northern and Southern Hemisphere with respect to the equator is called a cyclone pair (or a twin cyclone). Rare phenomena as they are, the cyclone pairs were already recognized in the last century (Reid, 1849) and are now observed much more explicitly by the meteorological satellites. Palmer (1952) described cyclone pairs are likely to occur in April, May, November and December. Keen (1982) indicated they are seldom observed during the northern summer season.

During the El Niño event which developed in the spring of 1991 and ceased in the summer of 1992, cyclone pair formation was frequently observed; on 7 May 1991, 27 September 1991, 18 November 1991, and 5 January 1992. Figure 1 shows the sea level wind and pressure analyses given by the operational global analysis of JMA at 24-hour intervals from 12 UTC on 31 December 1991 to 12 UTC on 11 January 1992. As presented in these figures, the analyses illustrate a cyclone pair occurrence and their movements towards the west. It should be noted that westerly winds began to strengthen on 2 January and two cyclones were generated north and south of the equator on 5 January with the outbreak of westerly bursts between these two systems. The northern system migrated towards the west subsequently followed by the southern one. Intensifying steadily, the northern system became Tropical Storm AXEL (9201) at 00 UTC 6 January and reached the peak intensity on the 8th, while the southern system became Tropical Cyclone BETSY and peaked on 10 January. The IR imagery of the cyclone pair taken by the GMS-4 at 12 UTC 8 January is shown in Figure 2. The cyclone in the southern hemisphere showed considerable intensification more than that in the northern hemisphere as indicated by the eye in the imagery. A cloud band formed over the equator corresponding to the strong westerly winds between the cyclones. In addition, the area of cloud clusters extended to the east of the cyclone pair, indicating active convection in the region.

As presented in the first article of this volume, bogus observations are assigned to make up for the data sparsity over the tropical ocean in the process of objective analyses at JMA (Ueno (1989)). In the present study no bogus observation was used, and nonetheless, the objective analysis provided reasonable tropical cyclone structures (Figure 1). It denotes that the data assimilation system of JMA has the capability of representing cyclone pairs, which is endorsed by Krishnamurti and Oosterhof (1989) who described that the resolution of about 100 km or finer is required for data assimilation systems to reasonably represent tropical cyclones.

3. Sea Surface Temperature

Figure 4 illustrates the distribution of sea surface temperatures (SSTs) and SST anomalies on 8 January 1992. Warm SSTs of 29°C or higher prevail around the date line in latitudes from the equator to 10°S, and positive SST anomalies are predominant east of the date line with maximums located over the equator from 150°W to 160°W. In Figure 4, corresponding to the warm SSTs east of the date line, deep convective clouds are found in that area, which exhibits enhanced convective activities there. Keen (1982) pointed out that low SOI (Southern Oscillation Index) with warm SSTs of 29°C or higher extending eastward across the date line encourages cyclone pair formation near the date line. Figure 4-(a) certainly illustrates the same SST pattern as indicated by Keen.

4. Cyclone Pairs and El Niño

Close relationships between cyclone pairs and El Niño have been discussed for the last decade. Ramage (1986) noted that cyclone pairs are crucial both in initiating and in prolonging El Niño. Miller et al. (1988) and Nitta (1989) suggested that the cyclone pair which occurred in May 1986 triggered the 1986-87 El Niño. In this case, the westerly bursts

associated with this cyclone pair induced Kelvin waves in the equatorial Pacific and generated an atmosphere–ocean coupling disturbance. Eventually, warm water piled in the equatorial Western Pacific was pushed towards the east and formed the typical SST pattern of El Niño.

For the 1991–92 El Niño, premonitory symptoms of the phenomenon had already been observed in early 1991, the events of cyclone pair in particular. In September 1991, JMA confirmed the occurrence of an El Niño event in accordance with the low SOI and the positive SST anomalies dominating over the Eastern and Central Pacific; the anomalous features of the SST resemble the conditions indicated by Keen (1982) as above. However, there was no evidence of eastward movement of the warm water in conjunction with the series of cyclone pair formation during the El Niño.

5 Prediction by the GSM

Figure 3 shows results of a series of operational prediction performed by the GSM for the same valid time, 12 UTC 8 January 1992, with initials at 12 UTC 7 January 1992 (1–day forecast) back to 12 UTC 31 December 1991 (8–day forecast). Compared with the analyses illustrated in Figure 1, these results indicate that the model successfully predicted the cyclones behavior in 1– to 4–day forecasts, whereas it produced increasing errors in positions and central pressures of the cyclones in 5– to 6–day forecasts, and ultimately failed in prediction in 7– to 8–day forecasts.

It is apparent this contrast in forecast performances is attributed to the difference in initials that definitely change at 12 UTC 3 January when the two cyclones are first identified (Figure 1). Namely, the cyclone pair was poorly represented in forecasts with initials at 12 UTC 3 January or earlier where cyclogenesis is not discernible, but it was well reproduced with initials at 12 UTC 4 January and later where an incipient disturbance is already embedded. The forecast failure as a result of having no embryo of disturbance in initial fields in this study holds true in the forecast of blocking in mid–latitudes.

6. Discussions and Remarks

The wind and pressure patterns derived by Gill (1980) and Zebiak (1982) in their studies to examine the atmospheric response to an equatorial heat source are quite similar to those patterns shown in Figure 1 (Lander 1990). Yamagata (1987) demonstrated that the burst of westerly winds, with the moisture convergence in front, generates wind and pressure patterns similar to those of cyclone pairs. Tropical atmosphere is naturally abundant in moisture supplied from the warm oceans below, whereas cyclone pairs are occasional events. It suggests that cyclone pairs require some inducements to be formed.

Madden and Julian (1971, 1972) found an atmospheric oscillation in equatorial regions that propagates eastward with 30–60 day period and zonal wave number 1. This 30–60 day oscillation in the tropics called the "Madden–Julian (MJ) oscillation" is closely linked with tropical cyclone activities (Nakazawa 1986; Storch and Smallegange 1992). Figure 5 presents the time–longitude cross section of 5–day mean velocity potential at 200 hPa for the eleven months from April 1991 to February 1992. We note that the MJ oscillation is delineated by eastward propagation of the velocity potential distributions at intervals of one to two months. Hatched are the areas with enhanced upper–level divergence associated with strong low–level

convergence and active convection. Indicated by "X" are the serial formations of a cyclone pair on 5 May 1991, 27 September 1991, 18 November 1991, and 8 January 1992. These cyclone pairs were fixed subjectively based on the global analysis and the satellite imagery. The figure depicts the eastward movements of active convection areas originating from 60°E and subsequent formations of cyclone pairs to the west of the date line.

Figure 6 shows the time–longitude cross section of the zonal wind anomaly at 850 hPa level as in Figure 5, where anomaly is defined as the deviation from longitudinal mean. Hatched areas indicate westerly bursts in the lower troposphere. Although the MJ oscillation is not clear in this figure, it is evident that cyclone pairs accompany westerly bursts. Accordingly, Figures 4 and 5 suggest that the MJ oscillation and associated westerly bursts gave some incentive to the formation of the cyclone pairs.

Considering that the socio–economic impact of El Niño is being significant, increasing emphasis should be laid on the improvement of numerical models' performance in the tropics. Currently, GSM is one of the few numerical models capable of predicting the MJ oscillation (Tsuyuki 1990). The MJ oscillation is no doubt closely related with the occurrence of tropical cyclones, while the cyclone pairs, the special forms of tropical cyclones, seem to play crucial roles in onset and development of El Niño.

Thus, the co–existence of phenomena with different scales in time and space together with their mutual interactions leads to the difficulty in numerical weather prediction. Although the El Niño and La Niña occurring in 2– to 3–year intervals are successfully simulated by several atmosphere–ocean coupling models, it is imperative to simulate phenomena with a time–scale of about one week including cyclone pairs for the prediction of the onset of El Niño.

REFERENCES

Bengtsson, L., 1993: Climate modeling at MPI/GERMANY. IAMAP/IAHS'93 Abstracts, M3–12.

Gill, A. E., 1980: Some simple solutions for heat–induced tropical circulation. *Quart. J. Roy. Meteor. Soc.*, **106**, 447–462.

Iwasaki, T., 1991: Status report on numerical prediction of typhoon. Proceedings of the Second Workshop for Natural Disaster Reduction. Karuizawa, Nagano, Japan, 23–27 September 1991, 250–258.

Keen, R. A., 1982: The role of cross–equatorial tropical cyclone pairs in the Southern Oscillation. *Mon. Wea. Rev.*, **110**, 1405–1416.

Krishnamurti, T. N. and D. Oosterhof, 1989: Prediction of the life cycle of a super typhoon with a high–resolution global model. *Bull. Amer. Meteor. Soc.*, **70**, 1218–1230.

Krishnamurti, T. N., D. Oosterhof and N. Dignon, 1989: Hurricane Prediction with a high resolution global model. *Mon. Wea. Rev.*, **117**, 631–669.

Lander, M. A., 1990: Evolution of the cloud pattern during the formation of tropical cyclone twins symmetrical with respect to the equator. *Mon. Wea. Rev.*, **118**, 1194–1202.

Madden, R. A. and P. R. Julian, 1971: Description of a 40–50 day oscillation in the zonal wind in the tropical Pacific. *J. Atmos. Sci.*, **28**, 702–708.

Madden, R. A. and P. R. Julian, 1972: Description of global–scale circulation cells in the

tropics with a 40–50 day period. *J. Atmos. Sci.*, **29**, 1109–1123.

Miller, L., E. Robert, E. Cheney and B. C. Douglas, 1988: GEOSAT altimeter observations of Kelvin waves and the 1986–87 El Niño. *Science*, 239, 52–54.

Nakazawa, T. 1986: Intraseasonal variations of OLR in the Tropics during the FGGE year. *J. Meteor. Soc. Japan*, **64** , 17–34.

Nitta, Ts., 1989: Development o a twin cyclone and westerly bursts during the initial phase of the 1986–87 El Niño. *J. Meteor. Soc. Japan*, **67** , 677–681.

Palmer, C., 1952: Tropical meteorology. *Quart. J. Roy. Meteor. Soc.*, **78**, 126–164.

Reid, W., 1849: *The law of storms*. Weale, London, 424pp.

Ramage, C. S., 1986: El Niño. *Scientific American*, **254**, No. 6, 55G–61.

Storch, H. von and A. Smallegange, 1991: The phase of the 30– to 60day oscillation and the genesis of tropical cyclones in the Western Pacific. Max–Plank–Institute für Meteorologie Report No. 66, 22pp.

Tsuyuki, T. 1990: Prediction of the 30–60 day oscillation with the JMA global model and its impact on extended–range forecasts. *J. Meteor. Soc. Japan*, **68** , 183–201.

Ueno, M., 1989: Operational bogussing and numerical prediction of typhoon in JMA. JMA/NPD Technical Report, No. 28, Japan Meteorological Agency, Numerical Prediction Division, Tokyo, 48pp.

Yamagata, T., 1987: A simple moist model relevant to the origin of intraseasonal disturbances in the Tropics. *J. Meteor. Soc. Japan*, **65**, 153–165.

Zebiak, S. E., 1982: A simple atmospheric model of relevance to El Niño. *J. Atmos. Sci.*, **39**, 2017–2027.

10 M/S

１２月３１日１２UT
GANAL SURF HPA

１月　１日１２UT
GANAL SURF HPA

１月　２日１２UT
GANAL SURF HPA

１月　３日１２UT
GANAL SURF HPA
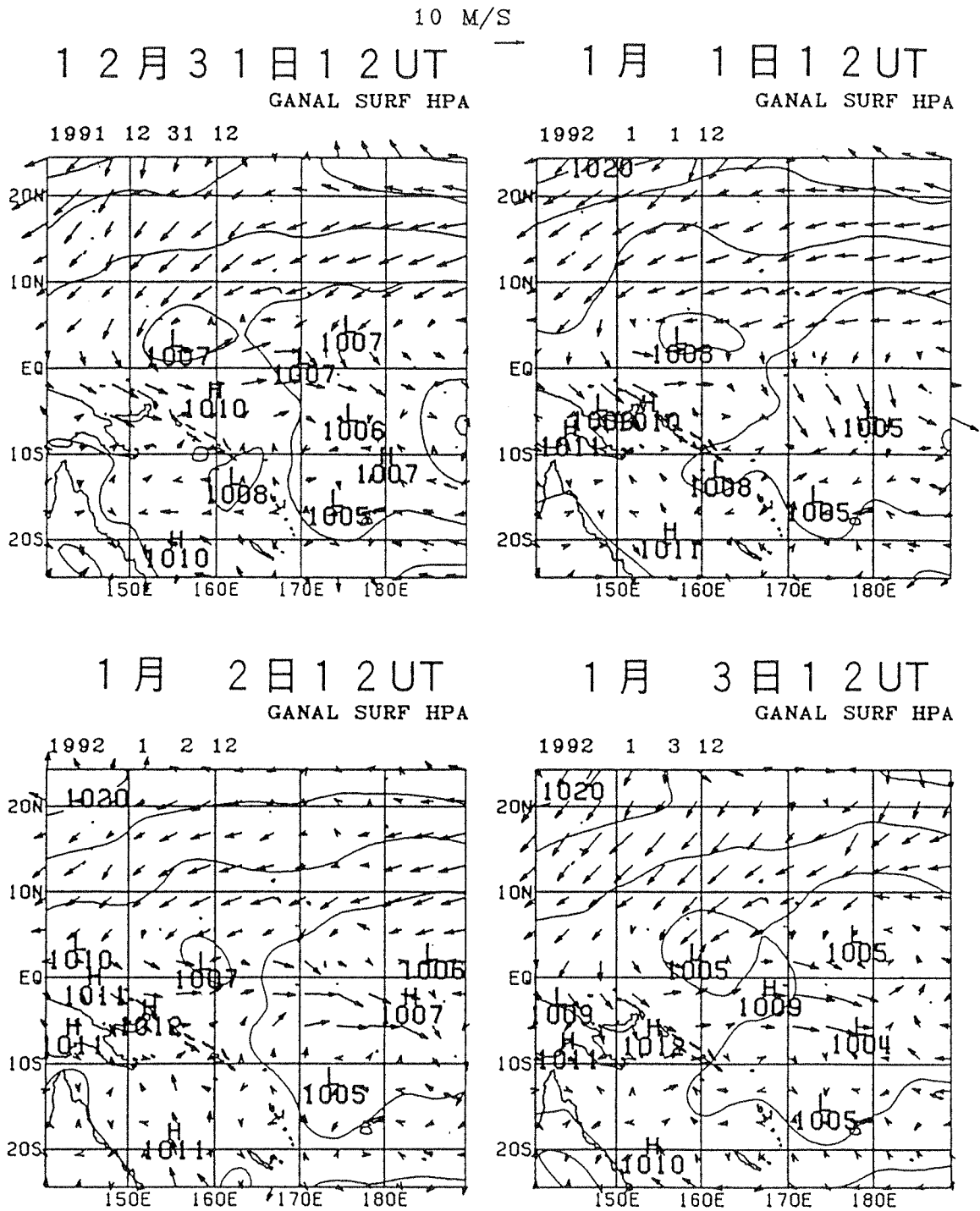
Fig. 1. The sea level wind and pressure analysis from 12 UTC 31 December 1991 to 12 UTC 11 January 1992.

10 M/S

1月 4日12 UT
GANAL SURF HPA

1992 1 4 12
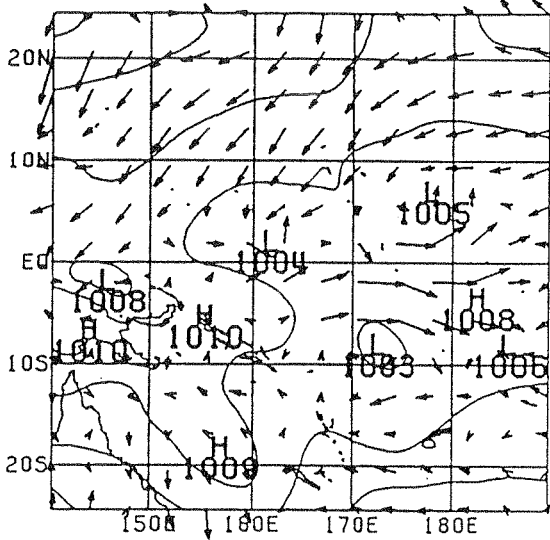
1月 5日12 UT
GANAL SURF HPA

1992 1 5 12
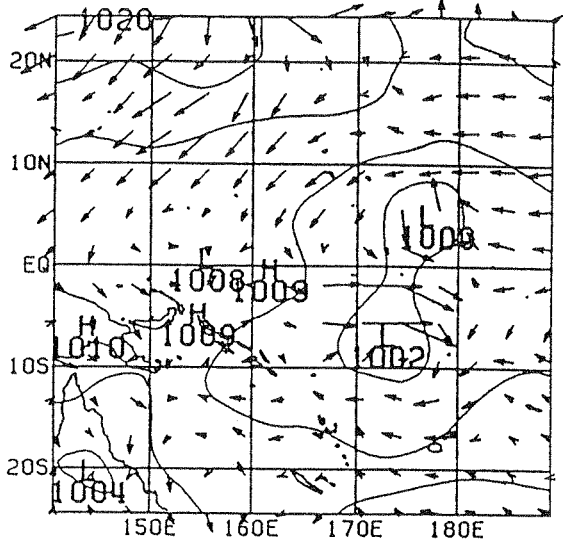
1月 6日12 UT
GANAL SURF HPA

1992 1 6 12
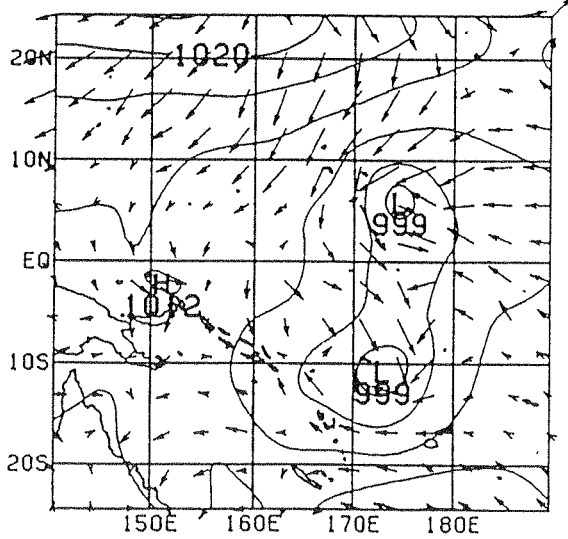
1月 7日12 UT
GANAL SURF HPA

1992 1 7 12
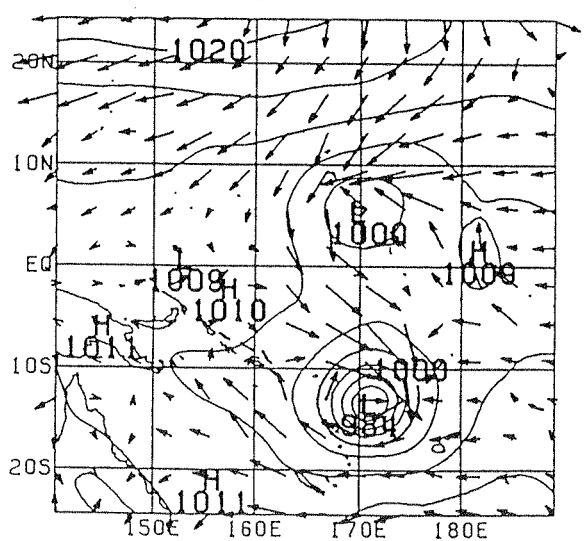
Fig. 1. (Continued)
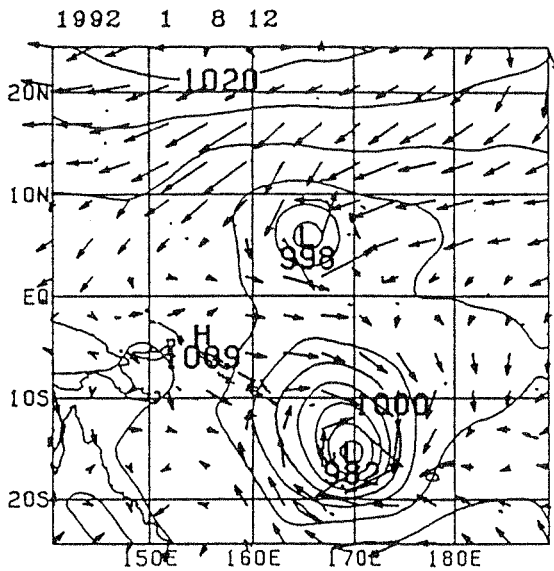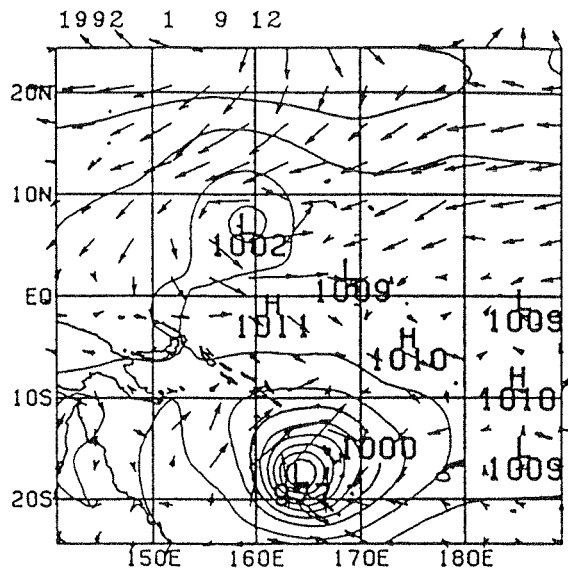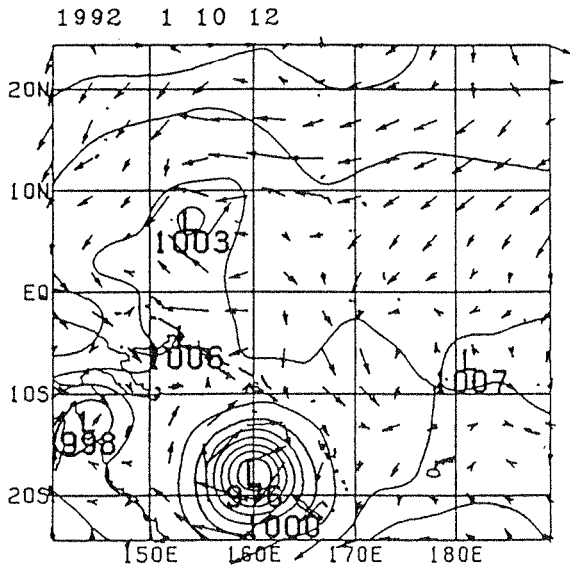
10 M/S

1月 8日12UT
GANAL SURF HPA

1992 1 8 12

1月 9日12UT
GANAL SURF HPA

1992 1 9 12

1月10日12UT
GANAL SURF HPA

1992 1 10 12

1月11日12UT
GANAL SURF HPA

1992 1 11 12
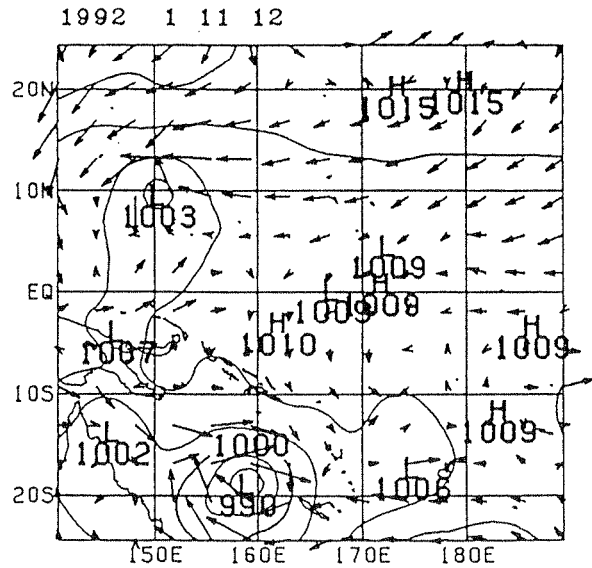
Fig. 1. (Continued)
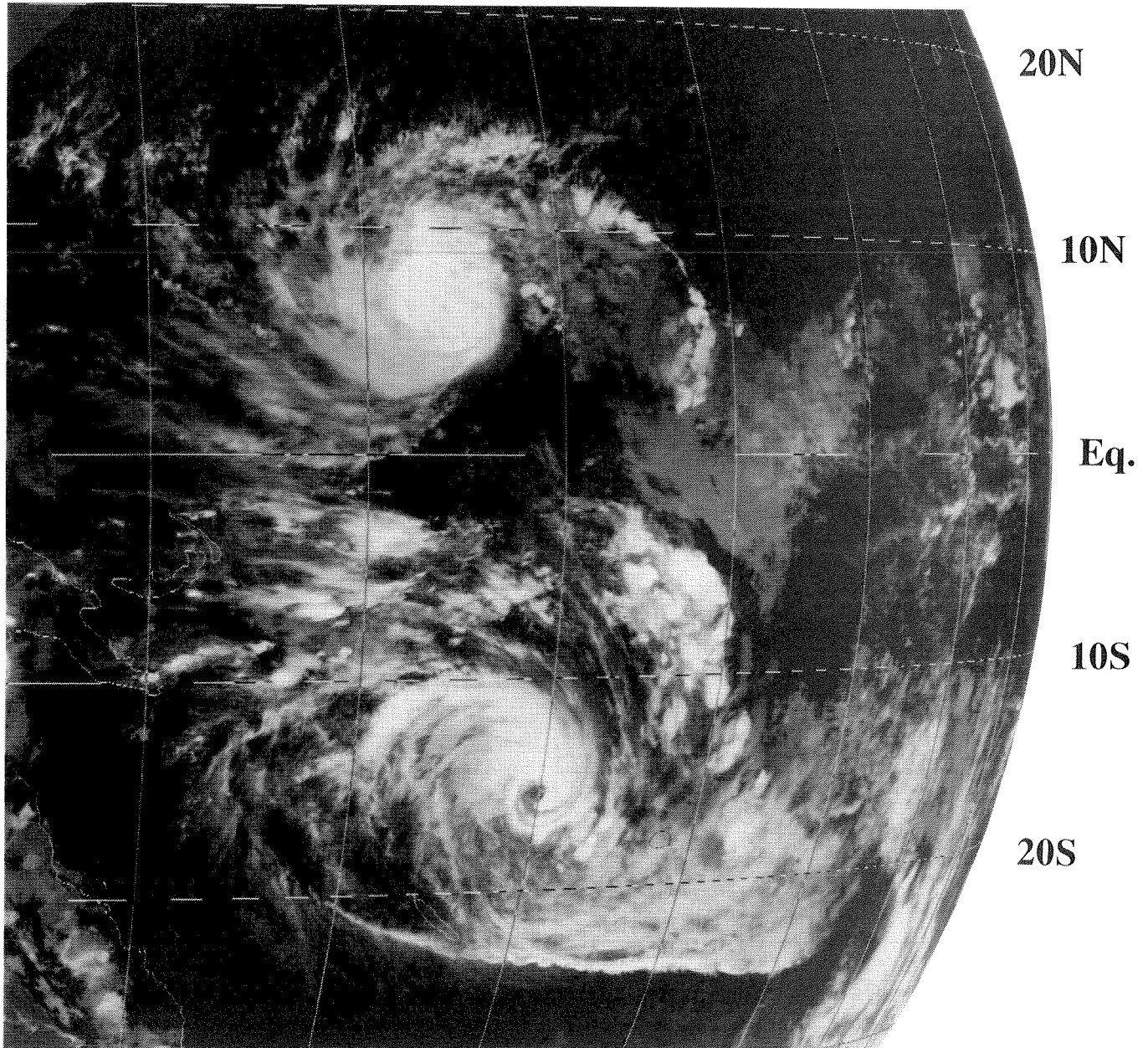
Fig. 2. Satellite image taken with GMS-4 at 12 UTC 8 January 1992.

10 M/S

1-day forecast

1992 1 7 12 INIT SURFACE
1992 1 8 12 VALID FT= 24

2-day forecast

1992 1 6 12 INIT SURFACE
1992 1 8 12 VALID FT= 48

3-day forecast

1992 1 5 12 INIT SURFACE
1992 1 8 12 VALID FT= 72

4-day forecast

1992 1 4 12 INIT SURFACE
1992 1 8 12 VALID FT= 96
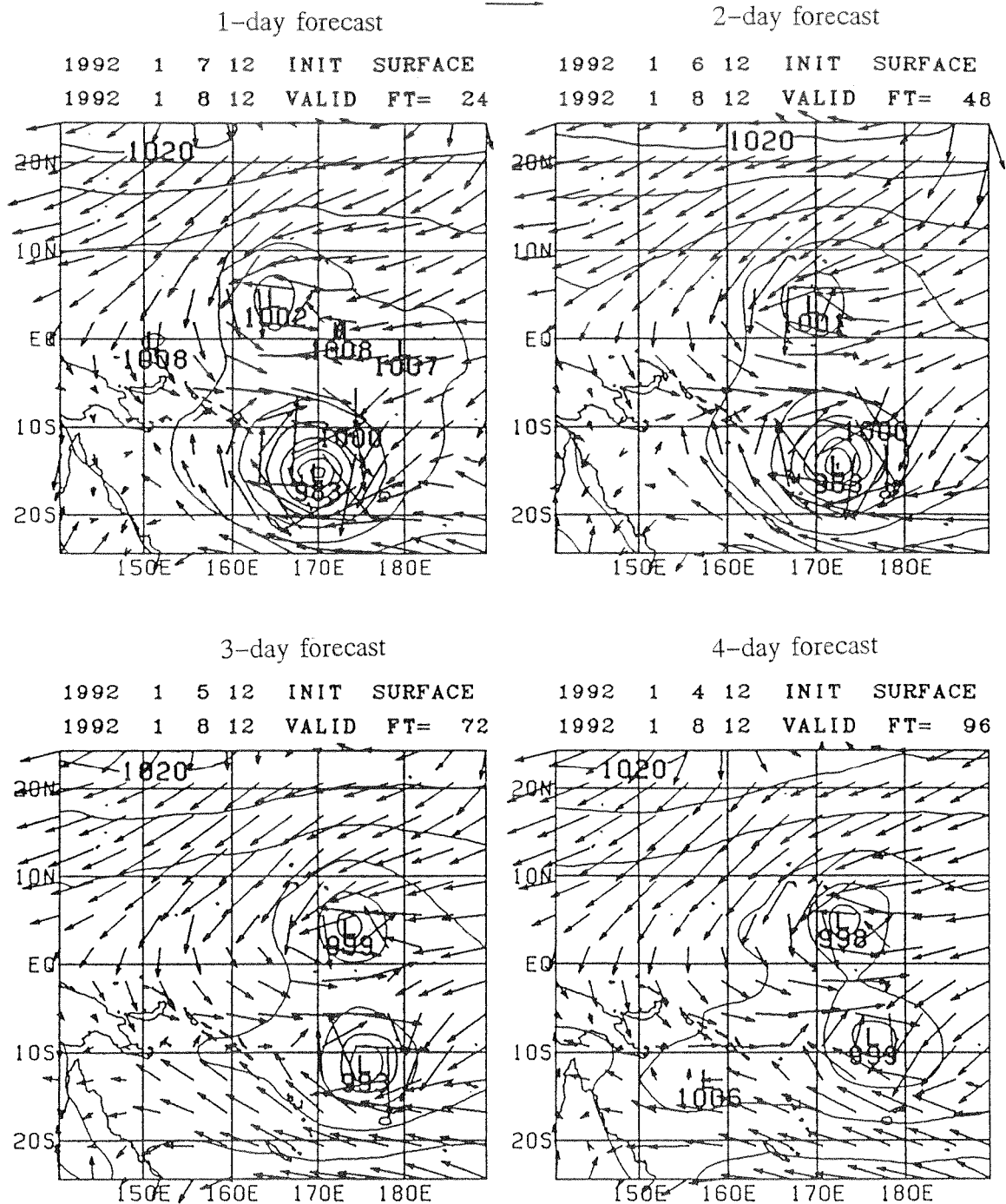
Fig. 3. Operational predictions by GSM for the valid time; 12 UTC 8 January 1992.

10 M/S

5-day forecast

6-day forecast

1992 1 3 12 INIT SURFACE
1992 1 8 12 VALID FT= 120
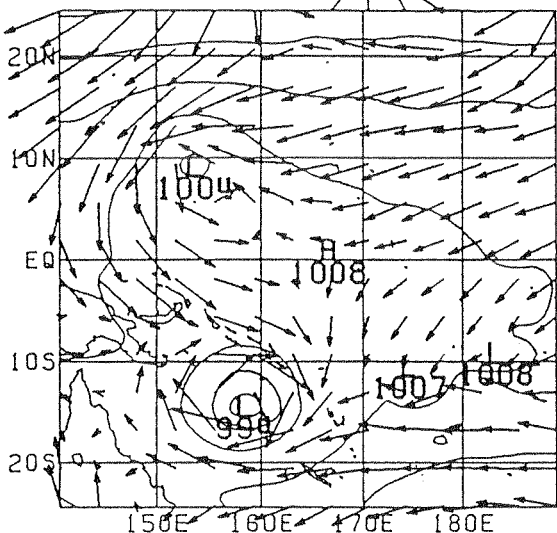
1992 1 2 12 INIT SURFACE
1992 1 8 12 VALID FT= 144
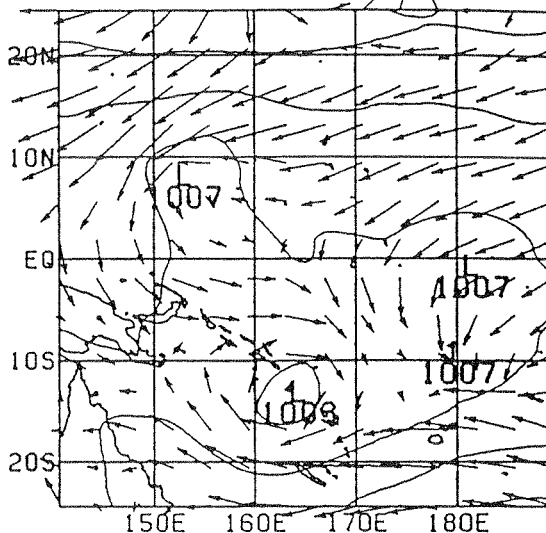
7-day forecast

8-day forecast

1992 1 1 12 INIT SURFACE
1992 1 8 12 VALID FT= 168
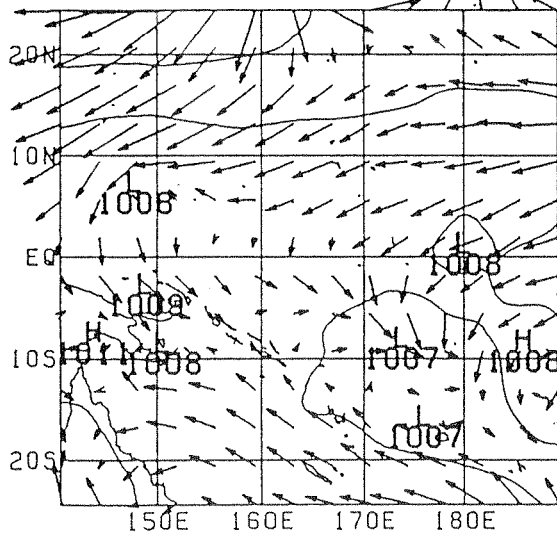
1991 12 31 12 INIT SURFACE
1992 1 8 12 VALID FT= 192
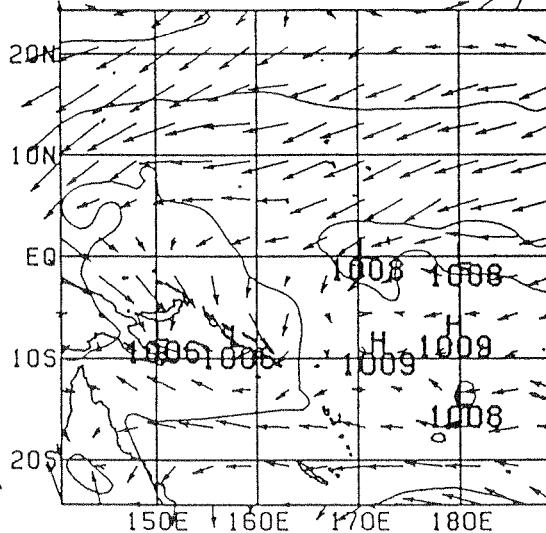
Fig. 3. (Continued)
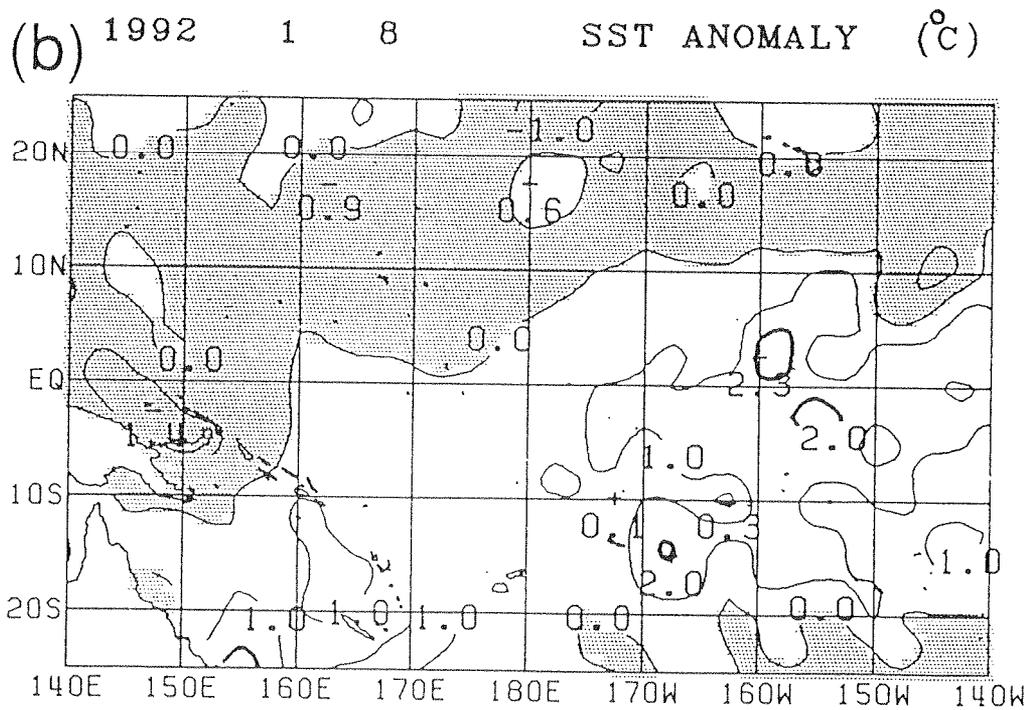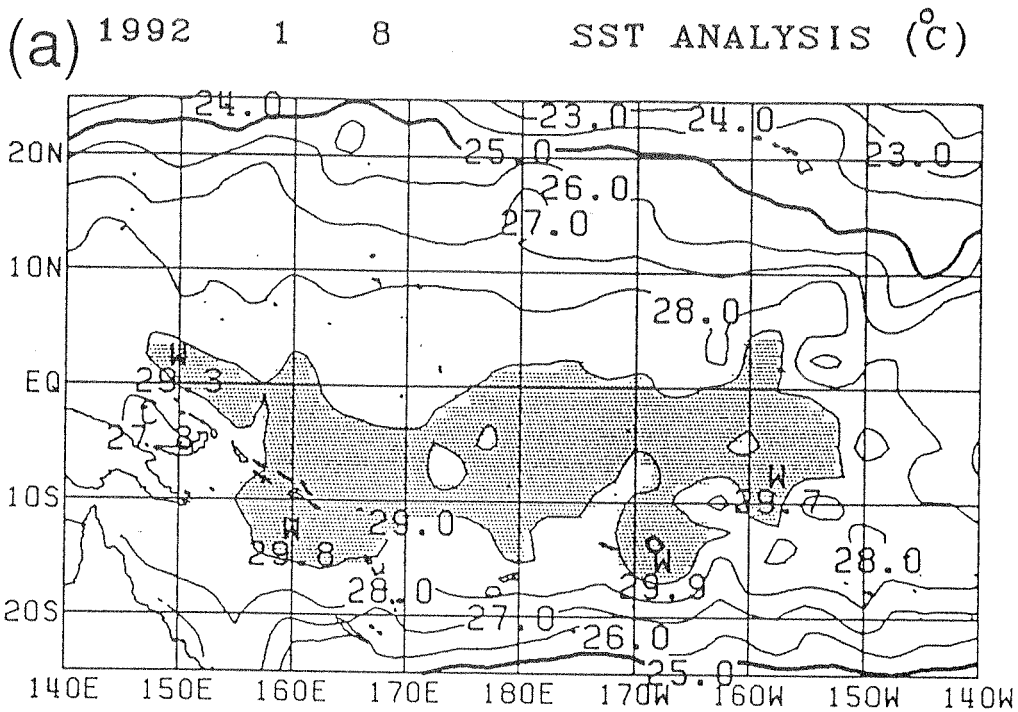
Fig. 4. Sea surface temperature (a) and its anomalies (b) for 12 UTC 8 January 1992.
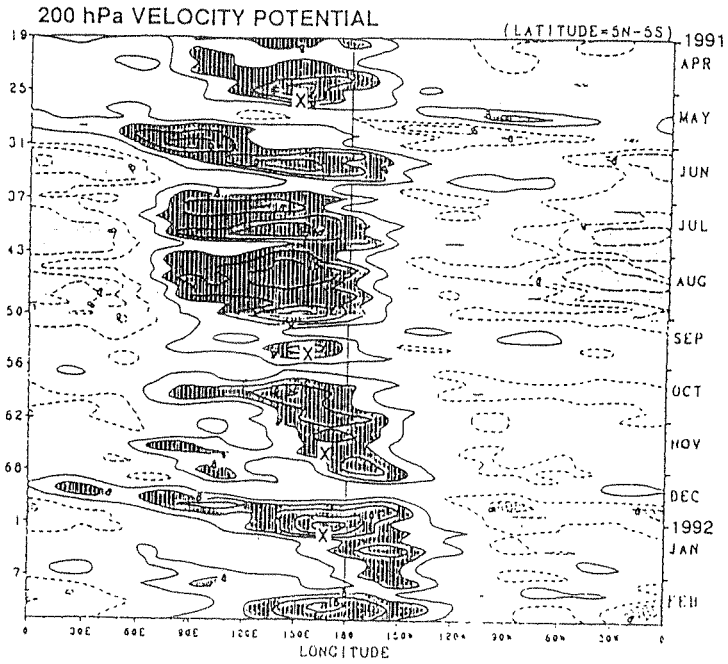
200 hPa VELOCITY POTENTIAL

Fig. 5. The time–longitude cross section of 5–day mean velocity potential at 200 hPa for eleven months from April 1991 to February 1992.

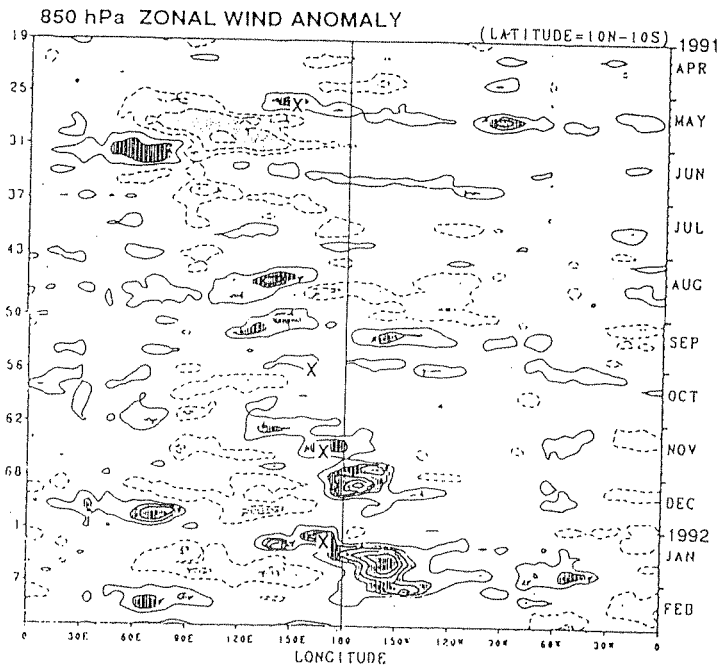## 850 hPa ZONAL WIND ANOMALY

Fig. 6. The time–longitude cross section of 5–day mean velocity potential at 850 hPa for eleven months from April 1991 to February 1992.